ISSN 0915-633X

NATIONAL INSTITUTE FOR FUSION SCIENCE

Net Current Increment of negative Muonlike Particle Produced by the electron and Posititve Ion Bunch-method

J. Uramoto

(Received - Nov. 5, 1997)

NIFS-527 Dec. 1997

RESEARCH REPORT
NIFS Series

NAGOYA, JAPAN

Net current increment of negative muonlike particle produced by the electron and positive ion bunch-method

Jōshin URAMOTO

National Institute for Fusion Science,
Oroshi-cho, Toki-shi, Gifu, 509-52, Japan

Abstract

In order to increase net currents of the negative pionlike π^- or muonlike μ^- particle under the method due to an electron and positive ion bunch, positive ions from the outside plasma must be supplied along the orbit of π^- or μ^- particle within the mass analyzer MA. This fact is proved experimentally by varying an injection position of the positive ion beam and the second electron beam to the analyzing magnetic field of MA, or by setting a metal plate which limits positive ions along the π^- or μ^- particle orbit. A theoretical net current as true negative pion or muon is estimated, which agrees roughly with the corresponding experimental value.

Keywords: apparent current, net current, positive ion

1. Introduction

On the productions of negative pionlike π^- or muonlike μ^- particles by the electron and positive ion bunch-method[1] and by the H_2 or D_2 gas discharge along magnetic field[2], it has been reported already that the apparent current of π^- or μ^- particle is much increased by supplying positive ions[3),4] in front of the beam collector BC of mass analyzer MA and by applying a positive bias voltage ($V_S > 0$) to BC. However, for practical applications, the net current of π^- or μ^- particle (when the beam collector bias voltage $V_S = 0$) is very important. In this paper, we will investigate some conditions to increase the net current of π^- or μ^- particle to BC in relation with the supply of positive ions along the orbit of π^- or μ^- particle within MA.

2. Ordinary experiment

Schematic diagrams of the experimental apparatus[1] are shown in Fig. 1 and Fig. 2. The first electron beam (F.E.B.) is stopped critically in front of the entrance slit S by an electrical potential of the decelerator D connected to the cathode of the electron gun. Next, a neutral gas is introduced into the first electron beam region and a plasma is produced through ionization of the gas. Then, positive ions of the plasma are accelerated in front of S, while a positive ion beam with an energy corresponding to the first electron beam acceleration voltage V_A is injected into the magnetic field region through S. Moreover, the stopped beam electrons are reaccelerated electrically toward the gap between two magnetic poles (N) and (S) through S, while the injected ion beam is decelerated electrically and stopped in the gap. The electrically reaccelerated electrons are injected perpendicularly to the magnetic field (B_M) and bunched in cyclotron motions of small radius.

As shown in Fig. 2, the above magnetic system is used as a mass analyzer (MA) of 90° type when the beam collector BC is arranged. The analyzing curvature radius r is 4.3 cm. It should be noted that the back space of the beam collector BC is surrounded by an insulator Ins. to interrupt the diffusion of positive ions from the secondary plasma S.P.[5]. This detection method of pionlike particles has reported already for the H_2 gas discharge plasma[6].

A fringe magnetic field distribution of the analyzing magnetic field B_M under a magnetic coil current of 1A, is shown in Fig. 3 for two different metal plates as the entrance plate (decelerator D) of Fig. 1 and Fig. 2. In this experiment, the iron (Fe) plate is used and the fringe magnetic field is much reduced.

The distribution of electrically applied potential are shown in Fig. 4. The first electron beam from the electron gun is perfectly reflected in front of the entrance slit S of the magnetic mass analyzer MA while a plasma is produced by a gas (air) ionization. Then, a positive ion beam is injected into MA through the slit S and the second electron beam is produced by reacceleration of the plasma electrons. It should be noted that the injected positive ion beam (i_2) is decelerated and stopped electrically, and that the second electron beam (e_2) suffers a magnetron (cyclotron) motion in the uniform magnetic field (which is used as the analyzing magnetic field of MA). As a result, both the electron beam and positive ion beam will be bunched within the small space at the entrance X of the uniform magnetic field.

Thus, we can expect a coherent interaction between the bunched electrons and positive ions.

For the first experiment of Fig. 2, dependences of a negative current I^- to the beam collector BC on the analyzing magnetic field B_M are shown in Fig. 5 for a first electron beam acceleration voltage V_A of 1 kV under a positive bias voltage V_S of the beam collector V_S = 100V. Here, we find that an analyzing relation of the negative muon μ^- is satisfied for the first peak of negative current I^-, if we assume that the effective acceleration voltage V_E is twice of the first electron beam acceleration voltage V_A. That is, the following relation is found: From the analyzing magnetic field B_M where the negative current shows a peak, the curvature radius r of the mass analyzer and the effective acceleration voltage V_E, we can estimate the mass m of the negatively charge particle by,

$$m = \frac{Ze\,(B_M r)^2}{2V_E}$$

$$= \frac{8.8 \times 10^{-2}\, Z\,(B_M r)^2\, m_e}{V_E}, \quad \cdots\cdots (1)$$

where e is the electron charge, B_M is in gauss unit, r is in cm unit, V_E is in volt unit and m_e is the electron mass and Z is the charge number. For the curvature radius r = 4.3 cm of this mass analyzer, the Eq. (1) is rewritten by

$$m = \frac{1.63\, Z\, B_M^2}{V_E} m_e. \quad \cdots\cdots (2)$$

From Eq. (2) and the experimental conditions for the first peak of I^- of Fig. 5, we obtain $m = m_1 \approx 200\ m_e$ under $V_E = 2V_A = 2$ kV and $B_M \approx 510$ gauss, assuming that $Z = 1$. This experimental result means that negative muonlike particles μ^- are produced (because the typical muon mass is near 207 m_e).

Moreover, we find the second peak of I^- in Fig. 5. From Eq. (2) and the experimental conditions, we obtain $m = m_2 \approx 285\ m_e$ under $V_E = 2$ kV and $B_M \approx 595$ gauss. This mass m_2 is near the typical pion mass (273 m_e). That is, negative pionlike particles π^- are produced also.

To investigate a relation between a net current and an apparent current of the π^- or μ^- particles to the beam collector BC, dependences of a negative current I^- to BC on the analyzing magnetic field B_M are determined in Fig. 6 under two bias voltages of $V_S = 0$V and $V_S = 100$V (at the first electron beam acceleration voltage $V_A = 1$ kV). In Fig. 6, we find that the peaks (corresponding to π^- or μ^-) of the negative current I^- increase about 60 times under the positive bias voltage $V_S = 100$V in comparison with that under $V_S = 0$V. These large apparent increments of negative current peaks under the positive potential $V_S > 0$ of the beam collector BC, have been explained by the positive ions in front of BC and secondary electrons inside BC[3].

3. Difference between two injection position

In the experiments up to now, a position Y_0 injecting the ion beam (I.B.) and the secondary electron beam (S.E.B.) as shown in Fig. 7 has been fixed at $Y_0 \approx 0.7$ cm within MA. The experimental results have been shown in Fig. 6 already for two beam collector bias voltages $V_S = 0$V and $V_S = 100$V.

Next, to adjust the supply of positive ions along the orbit of the π^- or μ^- particles within MA, another injection position Y_1 is determined at $Y_1 = 3.0$ cm as shown in Fig. 8. Thus, dependences of the beam collector current I^- on the analyzing magnetic field B_M are shown in Fig. 9 corresponding to Fig. 6 (the case of Y_0). Then, we find that the net current peak (at $V_S = 0$V) is much reduced to about 1/50 while the apparent current peak (at $V_S = 100$V) of μ^- is reduced by only about 1/3.5. We consider that the differences of I^- peaks between the two cases of Y_0 and Y_1 are caused by the differences of the supply of positive ions (+Ion) which come from the secondary plasma S.P. to the analyzing magnetic field region of MA as shown in Fig. 7 and Fig. 8. That is, the supply of positive ions along the orbit of π^- or μ^- particle is sufficient in the case of $Y_0 = 0.7$

cm and is not sufficient in the other case of $Y_1 = 3.0$ cm. This difference between the two cases of Y_0 and Y_1 becomes more clear when the first electron beam (F.E.B.) current I_A increases. In Fig. 10, dependences of I^- on B_M for Y_0 and Y_1 are shown under $I_A = 30$ mA at $V_S = 0$V. There, the peak current of I^- for Y_0 is proportional to I_A as understood from Fig. 6 while the other peak current of I^- for Y_1 is saturated. In conclusion, the net current of μ^- particle (at $V_S = 0$) depends on the positive ion supply along the orbit within MA while the apparent current (at $V_S > 0$) depends on the positive ion supply in front of BC.

4. Positive ion limit along orbit

As shown in Fig. 11, the positive ions along the orbit of π^- or μ^- particle are limited by setting a metal plate OMP. Thus, dependences of the negative currents I^- to BC on B_M are determined in Fig. 12 under $V_S = 0$ (net current) and $V_S = 100$V (apparent current). In comparison with the case of Fig. 6 (without OMP), the net current is much reduced below 1/50 while the apparent current stays about 1/10. Here, even if the first electron beam current I_A is increased to about 30 mA, the net current of μ^- particle is saturated below 0.02 μA.

5. Theoretical net currents

A net current as true negative pion (π^- meson) has been theoretically estimated[1] from a power balance and a cyclotron confinement of the injected electron beam: To produce one π^- meson, an energy of $E_\pi = 139.6$ MeV or 2.2×10^{-11} Joule is required for the electron beam. Thus, a net current I_t^- (μA) of the produced π^- meson is estimated from an effective electron beam power W_{ef} (W) injected into the mass analyzer, if the kinetic energy of π^- is neglected, by

$$I_t^- \approx \frac{eW_{ef}}{E_\pi}$$

$$= 7.1 \times 10^{-3}\ W_{ef}\ (\mu A). \quad \cdots\cdots (3)$$

When the π^- meson is detected at the beam collector position, the cyclotron radius of π^- is equal to the analyzing radius $r = 4.3$ cm of the mass analyzer. At this magnetic field intensity of the mass analyzer, the electron cyclotron radius is estimated to be about $r_e = 0.26$ cm from the

mass ratio of $m_2/m_e \approx 273$, if the π^- and the electron are accelerated at the same potential ($2\ V_A$). Then, the flight time of π^- from the production position X to the beam collector BC is $t_\pi = (2\pi r/4)/v_\pi$, where v_π is the velocity of π^-. During the flight time t_π, the number of the electron cyclotron motions are estimated to be $t_\pi/(2\pi r_e/v_e) = (1/4)\ (r/r_e)\ (v_e/v_\pi)$, where v_e is the electron velocity and $(2\pi r_e/v_e) = t_e$ means a time of one electron cyclotron motion. As the $(r/r_e)\ (v_e/v_\pi)$ is equal to the mass ratio $m_2/m_e = 273$, the number of electron cyclotron motion is determined to be about 68 times.

Here, if the cyclotron motions of about 68 times of the beam electrons inside the mass analyzer is considered as an energy multiplication due to a kind of confinement, Eq. (3) is rewritten by,

$$I_t^- \approx 5.5 \times 10^{-1}\ W_b\ (\mu A)$$

$$= 5.5 \times 10^{-7}\ I_b V_b\ (\mu A), \quad \cdots\cdots (4)$$

where W_b is an usual electron beam power (W unit), and I_b and V_b are the injected electron beam current (μA) and the effective electron beam acceleration voltage (V).

Another net current as negative true muon μ^- particle has been also estimated already[7]: To produce one negative true muon μ^- particle, an energy of $E_\mu = 105.7$ MeV or 1.7×10^{-11} Joule is required for the electron beam. Thus, a net current I_t^- (μA) of the produced true negative muons is estimated from an effective electron beam power W_{ef} (W) injected into the mass analyzer, if the kinetic energy of μ^- is neglected, by

$$I_t^- \approx \frac{eW_{ef}}{E_\mu}$$

$$= 9.4 \times 10^{-3}\ W_{ef}\ (\mu A). \quad \cdots\cdots (5)$$

At the productions of the μ^- particles, we can estimate that the electron cyclotron radius is about $r_e \approx r/14 \approx 0.3$ cm when the μ^- particles arrive at the beam collector position $r = 4.3$ cm (an analyzing radius of the mass analyzer), because the peak of μ^- appears at a magnetic field 14 times larger that for the electron beam. Then, the number of times of the electron cyclotron motions are

about 50 times, which are determined from (1/4) (r/r_e) (v_e/v_μ), where v_e and v_μ are the electron velocity and the μ^- particle velocity.

Here, if the cyclotron motions of about 50 times of the beam electrons inside the mass analyzer is considered as an energy multiplications due to a kind of confinement, Eq. (5) is rewritten by,

$$I_t^- \approx 4.7 \times 10^{-1} W_b \ (\mu A)$$

$$= 4.7 \times 10^{-7} I_b V_b \ (\mu A), \quad \text{..... (6)}$$

where W_b is an usual electron beam power (W unit), and I_b and V_b are the injected electron beam current (μA) and be effective electron beam acceleration voltage (V). As a result, the net current of μ^- particle is estimated to be almost the same with that of π^- particle. Thus, if our experimental conditions are adopted for Eq. (6), that is, $V_b = 2\ V_A = 2 \times 10^3$V ($V_A$ = 1 kV) and the injected electron beam current $I_b \approx 10^3$ μA (as about 1/3 of I_A = 3 mA) are used, we obtain the theoretical net current $I_t^- \approx 1.0$ μA while I_t^- is near the experimental net current (peak of I^- as μ^- particle in Fig. 6).

6. Consideration on some effect of the positive ions

It is an experimental fact that the positive ion supply along the μ^- or π^- particle orbit is very important to increase the net current increment of the μ^- particle. However, the experimental fact is not always related with a space charge neutralization of μ^- particle, because the net current of μ^- particle is too small to cause the self-space charge repulsion of μ^- particles. We consider that some elementary particle theory must be applied to explain the experimental fact. That is, the experimental fact is not explained from the classical charged particle theories.

7. Variation of additional potential $+V_A$

Up to this report, we have assumed that an effective acceleration potential V_E is twice of the applied acceleration potential V_A in order to explain the experimental values as the pionlike (π^-) or muonlike (μ^-) particle. However, we find that the V_E corresponding to the net current peak

approaches the V_A as seen in Fig. 6 while the positive ions are supplied along the orbit of μ^-. That is, the additional potential $+V_A$ as shown in Fig. 4 decreases when the positive ions increase along the particle orbit. The more precise mechanism for the $+V_A$ must be discussed in future.

References

1) J. Uramoto: National Institute of Fusion Science, Nagoya, Japan-Research Report, NIFS-277 (1994).

2) J. Uramoto: NIFS-377 (1995).

3) J. Uramoto: NIFS-512 (1997).

4) J. Uramoto: NIFS- To be reported.

5) J. Uramoto: NIFS-414 (1996).

6) J. Uramoto: NIFS-400 (1996).

7) J. Uramoto: NIFS-266 (1993).

Figure Captions

Fig. 1 and Fig. 2: Schematic diagrams of the experimental apparatus.

F: Filament as electron emitter. K: Cathode of electron gun. A: Anode of electron gun. V_A: Initial electron acceleration voltage. I_A: Total negative current. F.E.B.: First electron beam. G: Neutral gas. D: Decelerator of F.E.B. S: Entrance slit (3 mm × 10 mm). Ins: Insulator. I.B.: Ion beam. S.E.B.: Second electron beam. e: Electrons with cyclotron motions. μ^-: Negative muonlike particle. (MA): Mass analyzer. Fe: Iron. C: Magnetic Coil. (N): North pole of electro-magnet. (S): South pole. B_M: Analyzing magnetic field. BC: Beam collector. I^-: Negative current to BC. V_S: Bias voltage of BC with respect to mass analyzer body. S.P.: Secondary plasma inside (MA). X: Entrance of uniform magnetic field. i: Ion bunch. π^-: Negative pionlike particle. +Ion: Positive ion.

Fig. 3 Fringe magnetic field distribution (at 1A of magnetic coil current).

B_M: Analyzing magnetic field of (MA). B_O: Uniform magnetic field inside (MA). X: End of uniform magnetic field. S: Entrance slit position. Fe: Magnetic field distribution in a case using iron plate as D in Fig. 1. Cu: Magnetic field distribution in a case using copper plate as D in Fig. 1.

Fig. 4 Applied electrical potential distribution

V: Electrical potential. V_A: Initial potential (voltage) of electron gun anode. V_E: Effective potential for μ^- (negative muonlike particle) and π^- (negative pionlike particle). e_0: Initial electrons from electron gun cathode. e_1: First electron beam. e_2: Second electron beam. i_1: Positive ion beam from plasma. i_2: Second positive ion beam. e–B: Electron bunch due to magnetic cyclotron motion. i–B: Positive ion bunch due to electrical retardation. K: Cathode position of electron gun. A: Anode position of electron gun. S: Slit position of mass analyzer. X: Entrance position of analyzing uniform magnetic field. $+V_A$: Additional potential generated by stopping the positive ion beam.

Fig. 5 Dependence of the negative beam collector current I^- on the analyzing magnetic field B_M under the initial electron acceleration voltage $V_A = 1$ kV and the total anode current $I_A = 3$ mA.

Beam collector bias voltage $V_S = 100$V. Neutral gas pressure is 1×10^{-4} Torr (Ar gas) in the first electron beam region. μ^-: (means negative muonlike particle). π^-: (means negative pionlike particle). e: (means electron).

Fig. 6 Dependences of I^- on B_M under $V_A = 1$ kV and $I_A = 3$ mA.

(1): $V_S = 0$V. (2): $V_S = 100$V.

Fig. 7 Ordinary injection position of positive ion beam and secondary electron beam.

Y_0: 0.7 cm. +Ion: Positive ions which come from the secondary plasma S.P..

(See captions of Fig. 1 and Fig. 2).

Fig. 8 New injection position Y_1: 3.0 cm.

(See captions of Fig. 1 and Fig. 2, and Fig. 7).

Fig. 9 Dependence of I^- on B_M under $V_A = 1$ kV and $I_A = 3$ mA at new injection position $Y_1 = 3.0$ cm.

(1): Beam collector bias voltage $V_S = 0$V. (2): $V_S = 100$V.

(See captions of Fig. 5 also).

Fig. 10 Comparison between I^- characteristic at Y_0 and I^- characteristic at Y_1 under $I_A = 30$ mA.

Y_0: Ordinary injection position. Y_1: New injection position.

Fig. 11 Schematic diagram with a metal plate OMP which limits positive ions along the orbit of π^- or μ^-.

Y_0: 0.7 cm.

(See captions of Fig. 1, Fig. 2 and Fig. 7)

Fig. 12 Dependence of I^- on B_M under limit of positive ions by a metal plate OMP.

Y_0: 0.7 cm. $V_A = 1$ kV and $I_A = 3$ mA. (1): $V_S = 0$V (net current). (2): $V_S = 100$V (apparent current).

Appendix

For the π^- or μ^- particles extracted from the H_2 gas discharge as shown in Figs. A1 (A) and A1 (B), it has been reported[3] that the apparent current of π^- or μ^- particle to BC of MA increases extremely when the positive ions are supplied in front of BC through scattering H^- ions by the back metal plate BMP as shown in Fig. A1 (B). However, the positive ions are not supplied along the π^- or μ^- particle orbit within MA as the secondary plasma S.P. under the electron and positive ion bunch-method does not exist around the analyzing magnetic iron. Therefore, the net current of the π^- or μ^- particles in this low energy (800 eV) will be limited to some small value because of the lack of positive ions and will not depend on the injection position Y as shown in Fig. A1 (B). In fact, both the apparent currents (at V_{BC} = 75V) and the net currents (at V_{BC} = 0V) of the π^- or μ^- particle do not depend on the injection position Y as shown in Figs. A2 (A) and (B) even if Y is varied from 0.7 cm to 3.0 cm. Moreover, the net currents remain to the small currents.

Figure Captions of Appendix

Fig. A1 (A) Schematic diagram of experimental apparatus.

1: Cylindrical plasma in discharge anode. 2: Discharge cathode. 3: H_2 gas flow. 4: Discharge power supply. 5: Electron acceleration power supply. 6: Vacuum pump. 7: Area where cylindrical plasma is transformed into sheet plasma. 8: Insulation tube. 9: A pair of permanent magnets. 10: Magnetic field coils. 11: Electron acceleration anode. I_A: Current to electron acceleration anode. CP: Cylindrical plasma. SP: Sheet plasma. B_Z: Magnetic field. L: First extraction electrode. M: Second extraction electrode. E: Final extraction electrode. V_M: Potential (variable) of second extraction electrode with respect to electron acceleration anode. V_E: Potential (800V) of final extraction electrode with respect to electron acceleration anode. MA: Magnetic deflection (90°) mass analyzer. B_M: Magnetic field intensity of MA. BC: Beam collector of MA. V_{BC}: Positive potential of BC with respect to MA. I^-: Negative current to BC. $H\bar{0}$: Hydrogen negative ions outside of sheet plasma. H^-: Accelerated hydrogen negative ions. $\pi\bar{0}$: Negative pionlike particles outside of sheet plasma. π^-: Accelerated negative pionlike particles.

Fig. A1 (B) Schematic diagram of mass analyzer.

S: Entrance slit position. X: Entrance of uniform magnetic field.

Ins: Insulator behind BC. +Ion: Positive ions in front of BC. Fe: shows Iron. Y: Injection position to analyzing magnetic field.

Fig. A2 (A) Dependences of negative current I^- to BC on magnetic field intensity B_M of MA under beam collector potential $V_{BC} = 0V$.

(1): Potential of second extraction electrode $V_M = 300V$. (2): $V_M = 75V$. H^-: Peak of I^- corresponding to hydrogen negative ion. π^-: Peak of I^- corresponding to negative pionlike particle. μ^-: Peak of I^- corresponding to negative muonlike particle. e_H: peak of I^- corresponding to high energy electron. Y: Injection positions.

Fig. A2 (B) Dependence of I^- to BC on B_M of MA under V_{BC} = 75V.

(1): V_M = 300V. (2): V_M = 75V H^-, π^-, μ^-, e_H: See captions of Fig. A2 (A). Y: Injection positions.

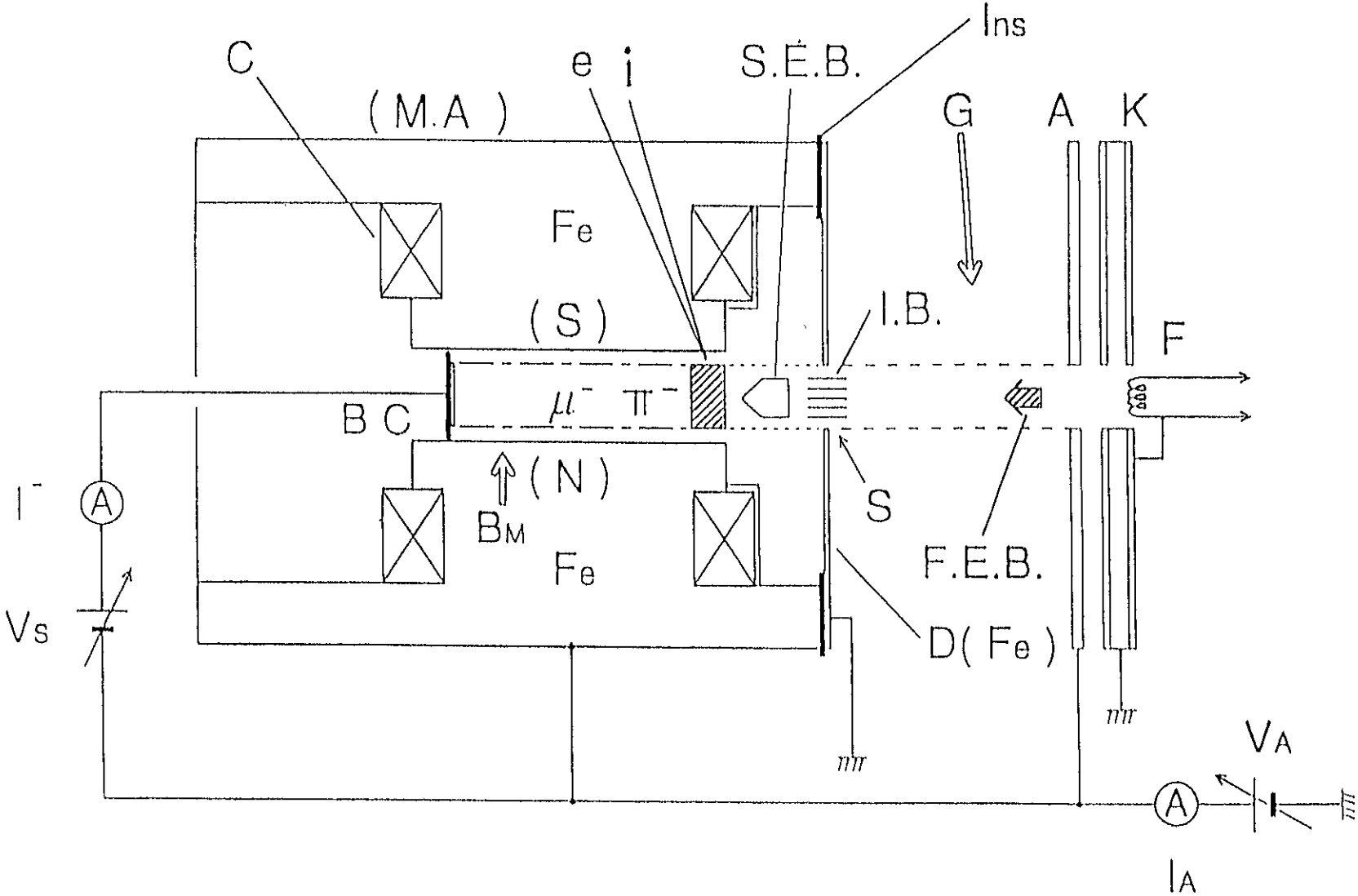

Fig. 1

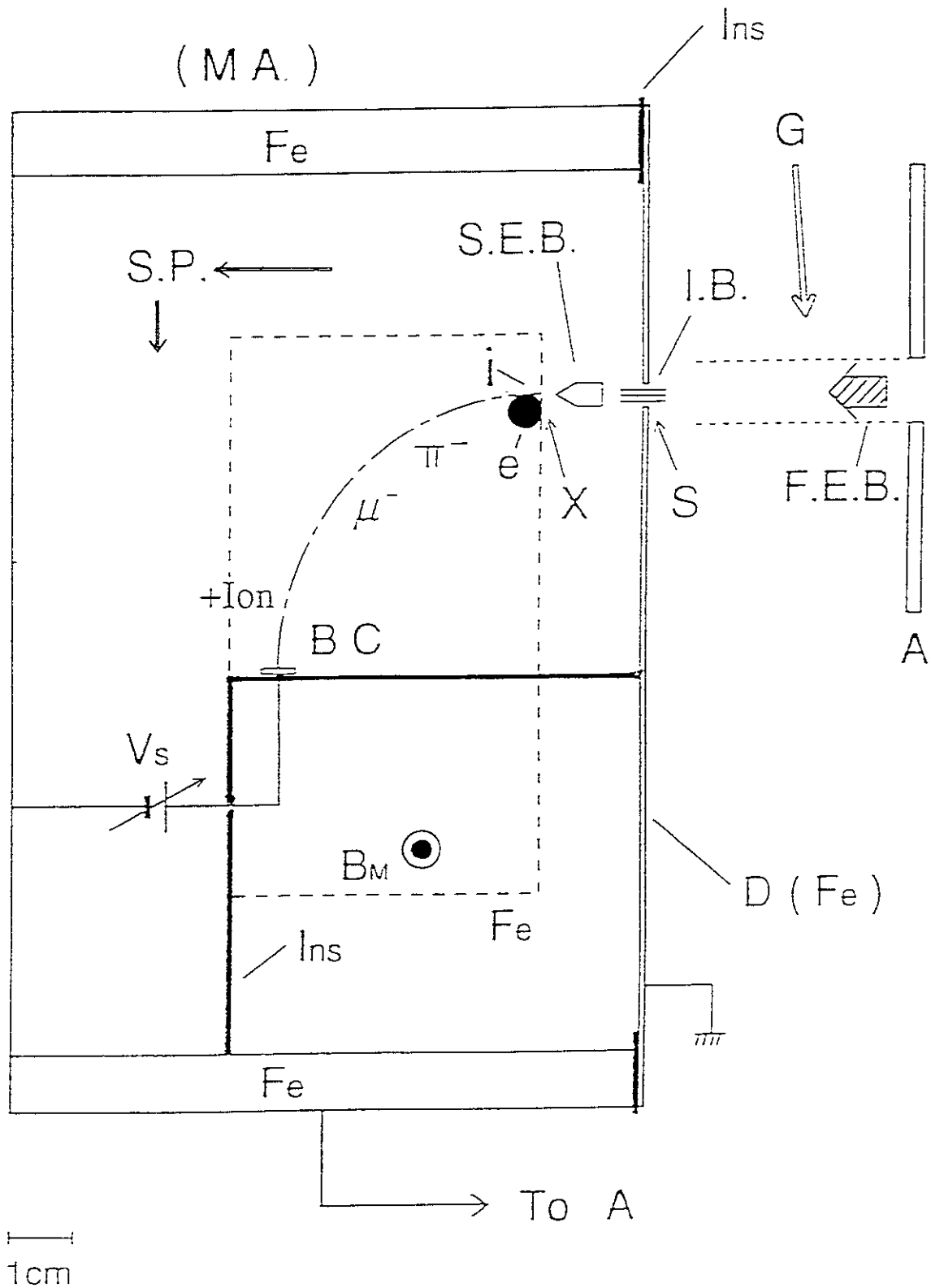
Ins
(M A.)
Fe
G
S.E.B.
S.P.
I.B.
i
π⁻
e
μ⁻
X
S
F.E.B.
+Ion
B C
A
Vs
BM
D (Fe)
Fe
Ins
Fe
To A
1cm

Fig. 2

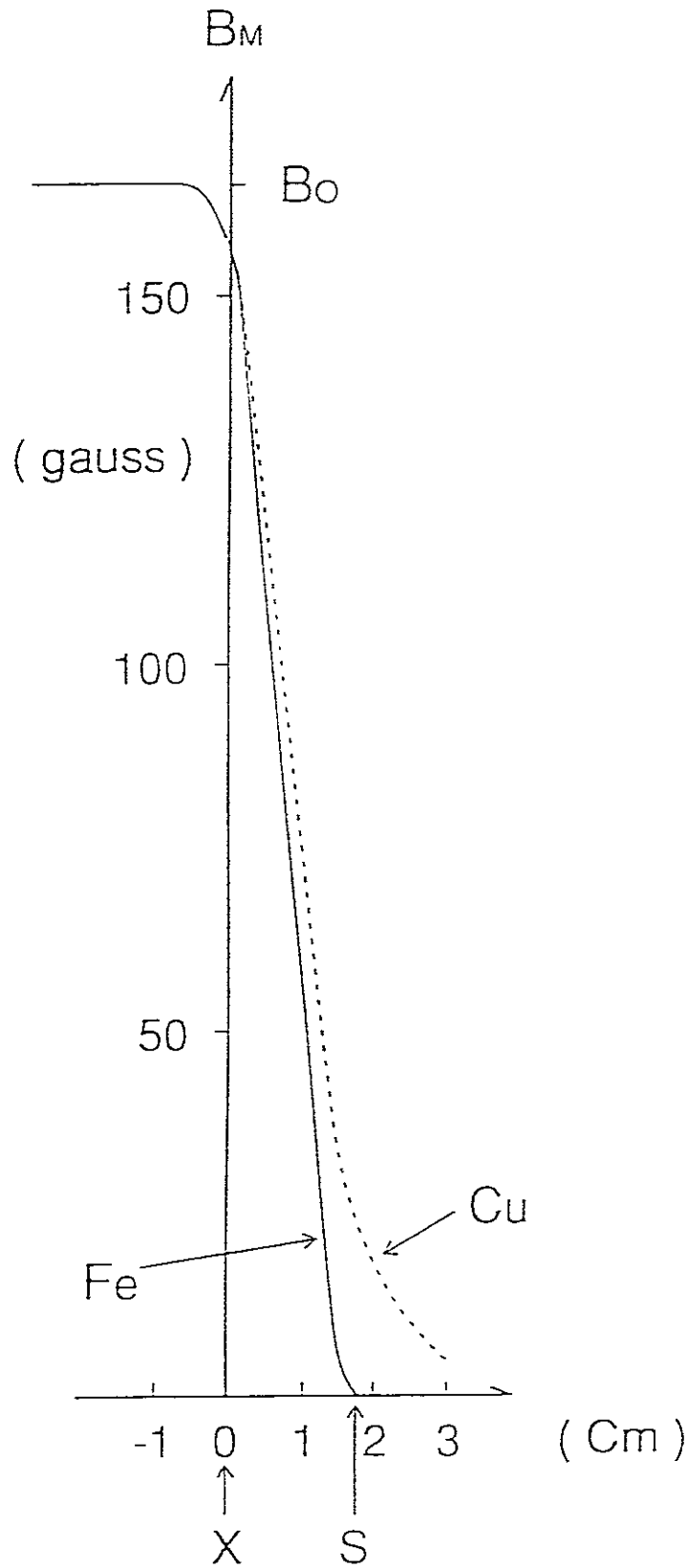

Fig. 3

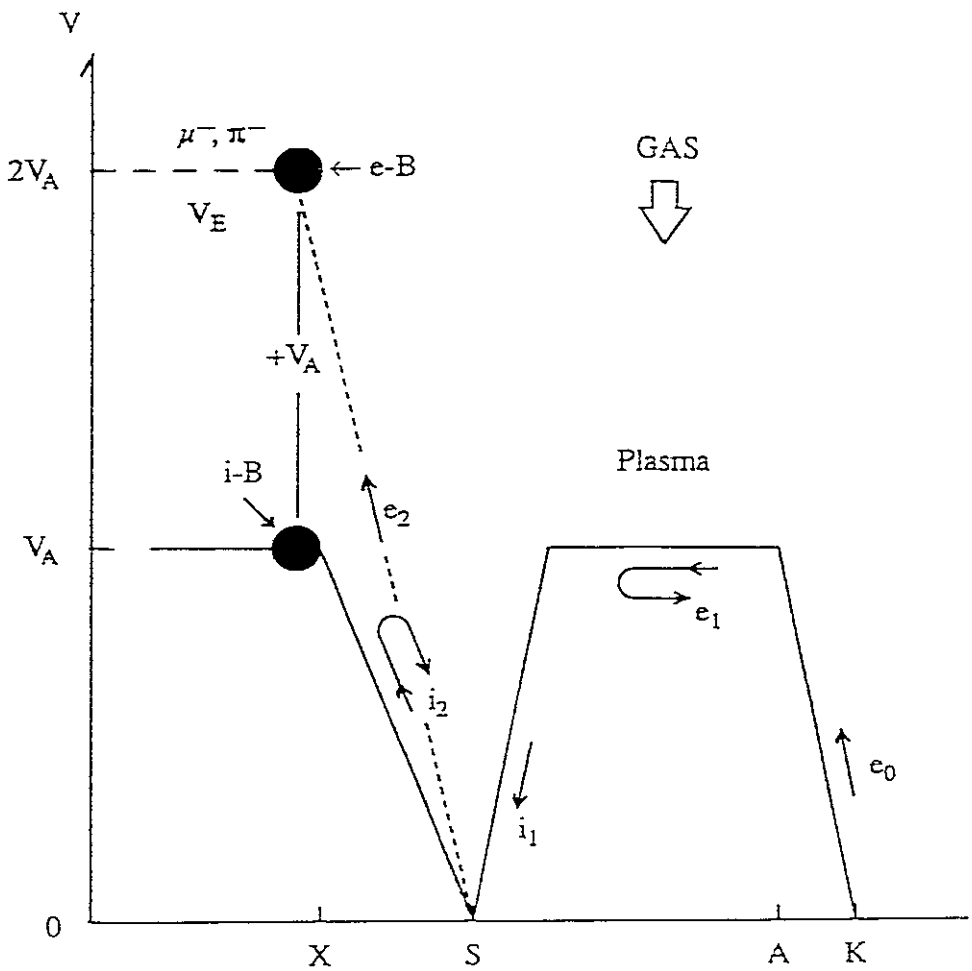

Fig. 4

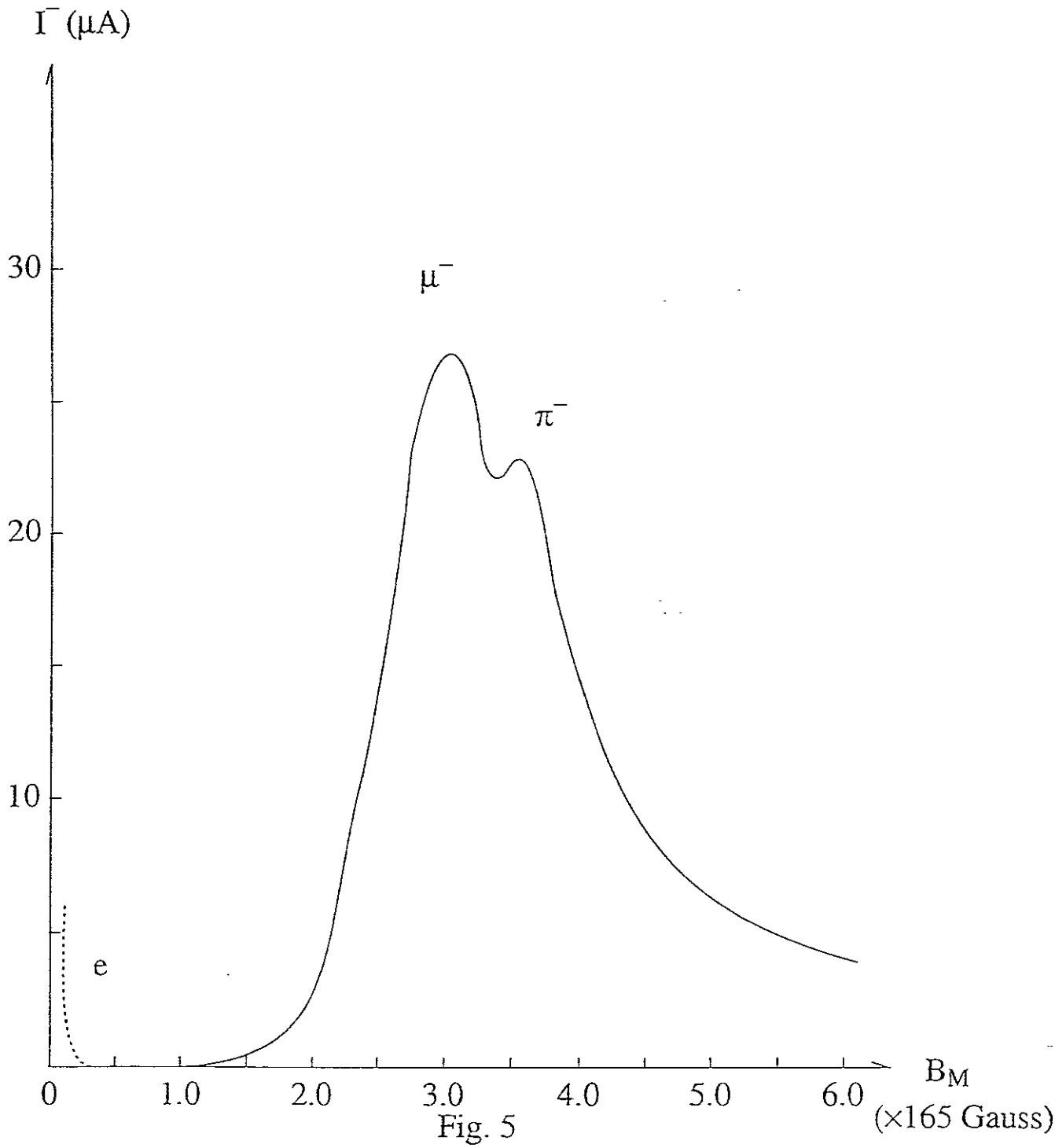

Fig. 5

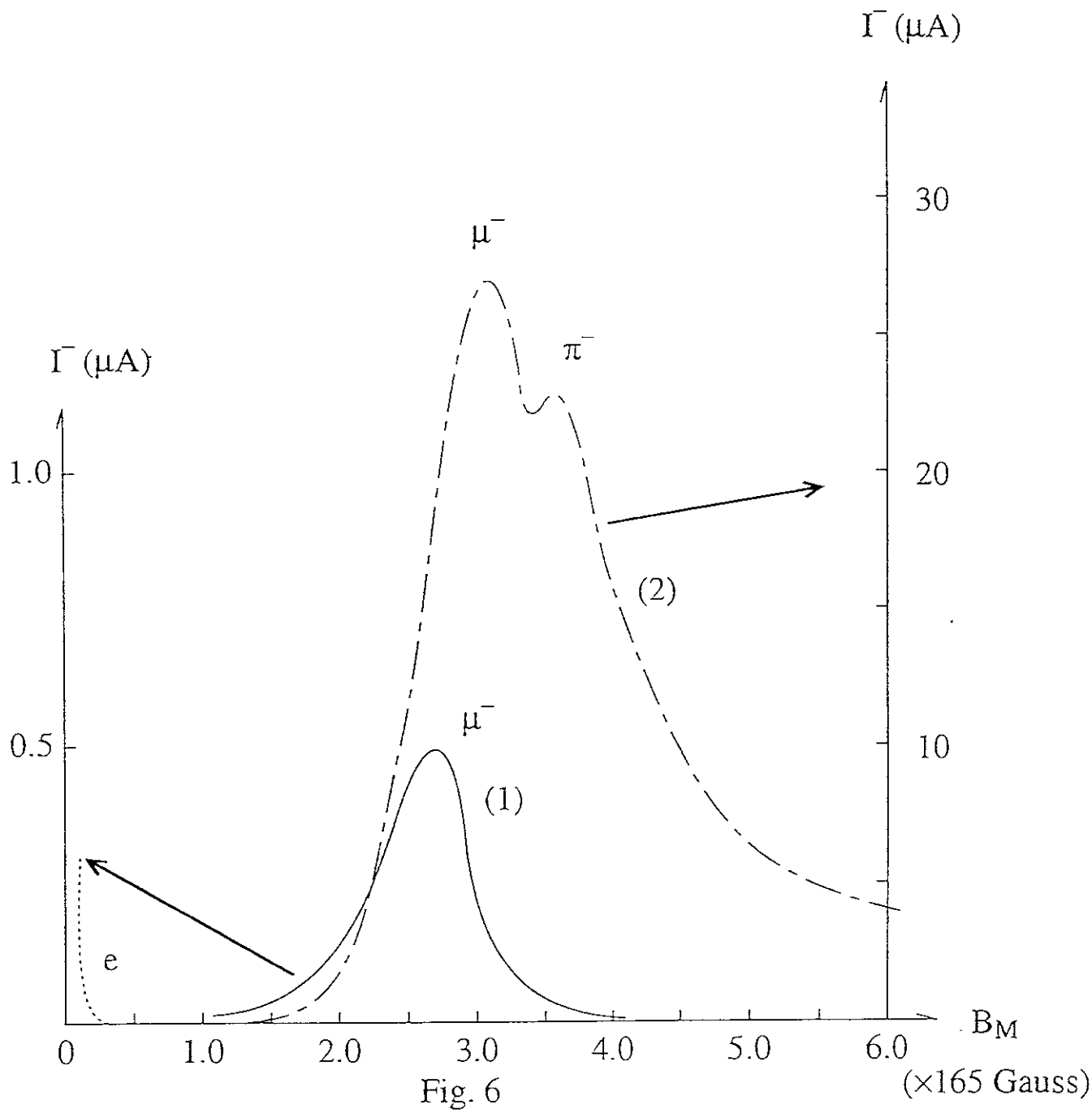

Fig. 6

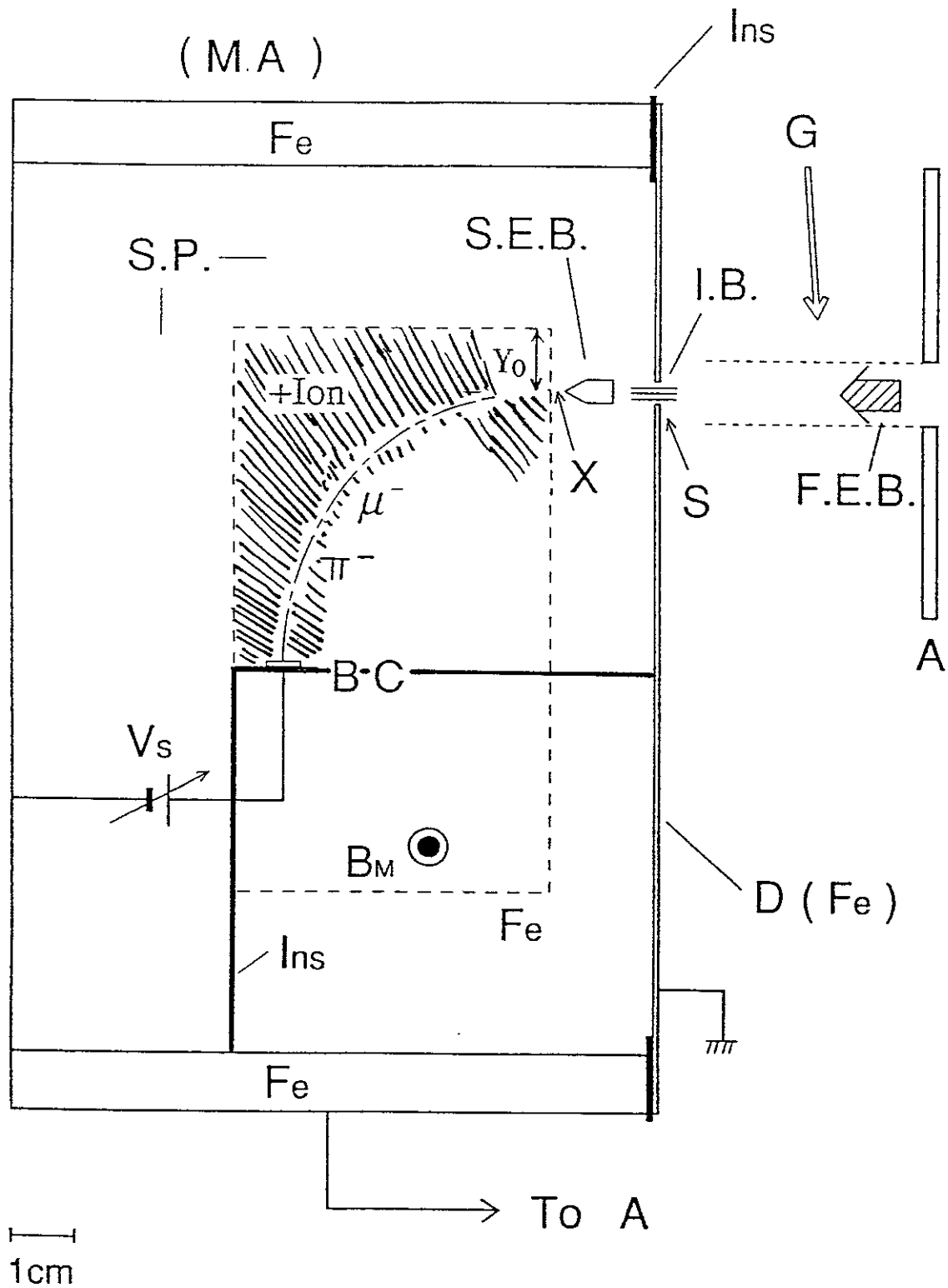
(M.A)
Ins
Fe
G
S.P.
S.E.B.
I.B.
Y0
+Ion
X
S
F.E.B.
μ⁻
π⁻
A
B-C
Vs
BM
D (Fe)
Fe
Ins
Fe
To A
1cm

Fig. 7

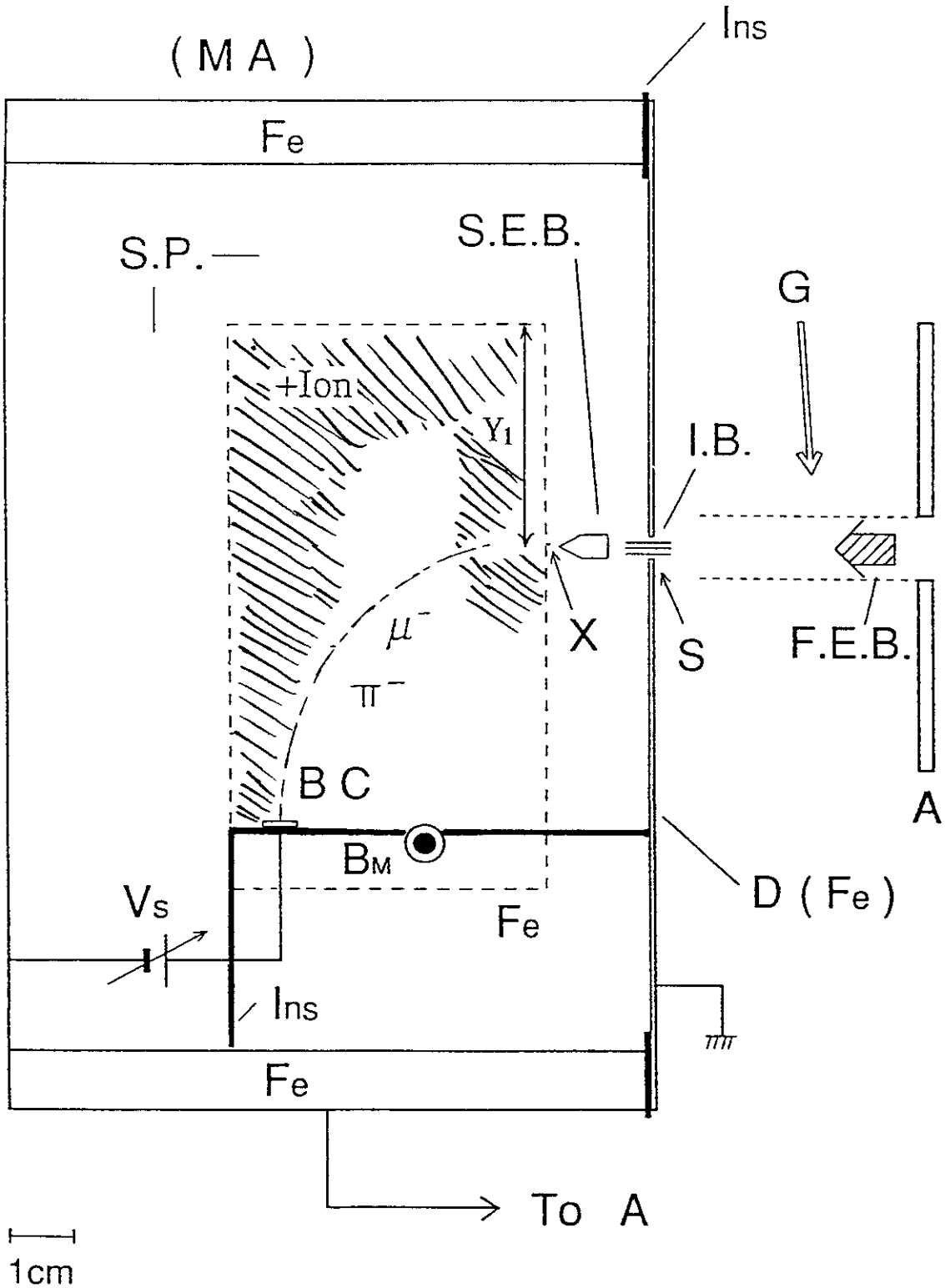
(M A)
Ins
Fe
S.P.
S.E.B.
G
+Ion
Y1
I.B.
X
S
F.E.B.
μ⁻
π⁻
B C
A
BM
D (Fe)
Vs
Fe
Ins
Fe
To A
1cm

Fig. 8

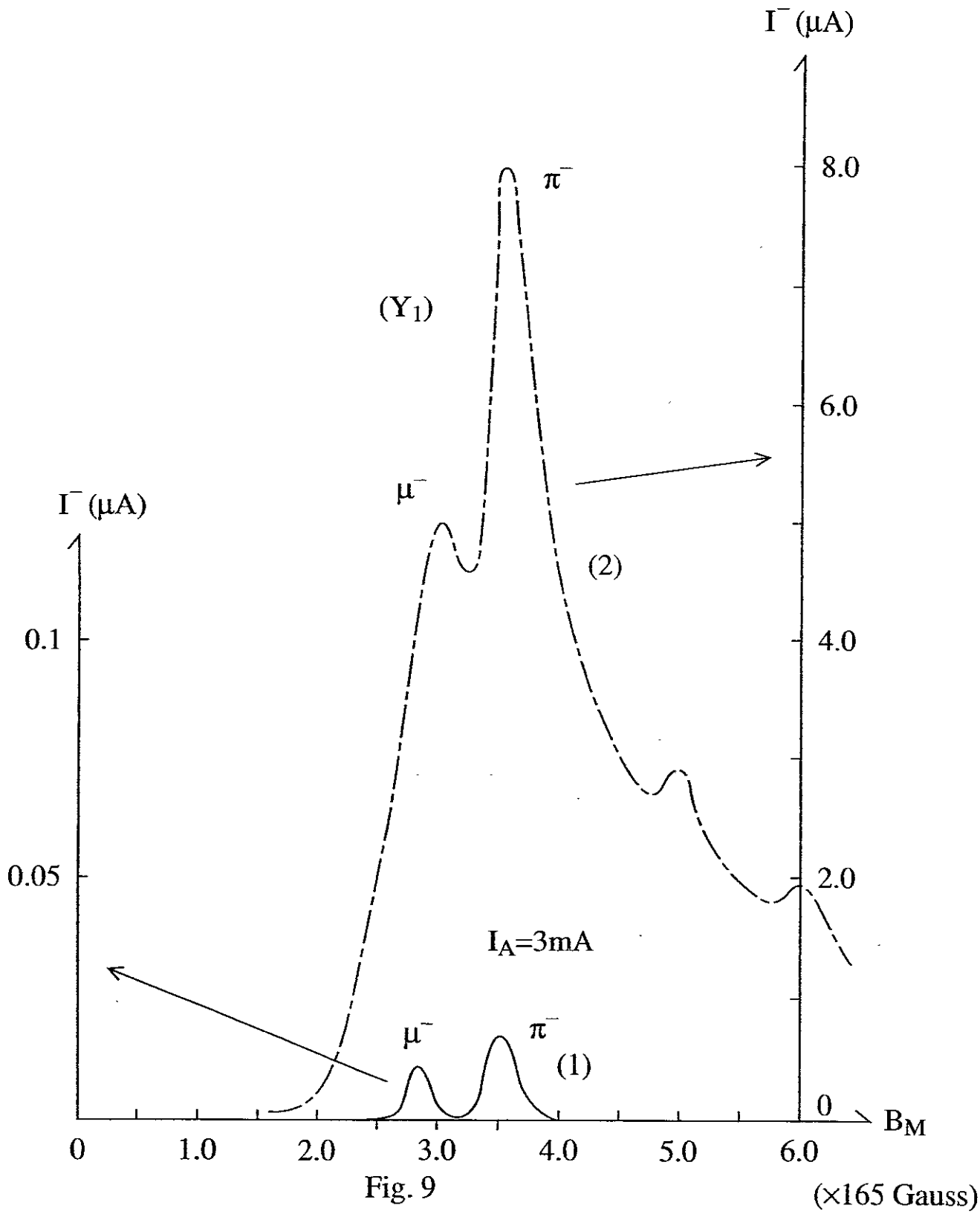
I⁻ (μA)
8.0
6.0
4.0
2.0
0
π⁻
(Y1)
μ⁻
(2)
I⁻ (μA)
0.1
0.05
IA=3mA
μ⁻
π⁻
(1)
0
1.0
2.0
3.0
4.0
5.0
6.0
BM
(×165 Gauss)

Fig. 9

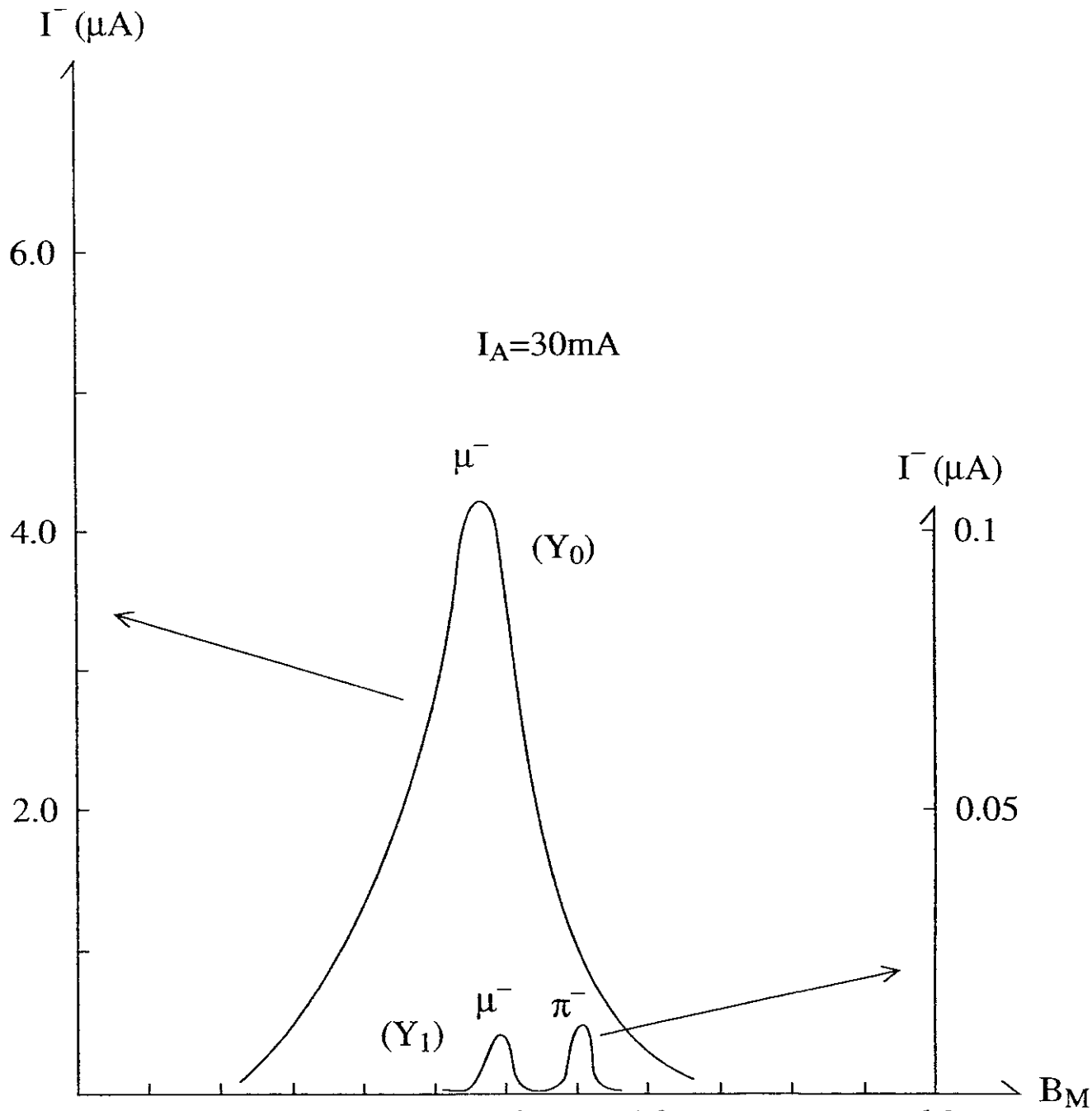
I⁻ (μA)
6.0
4.0
2.0
I_A=30mA
μ⁻
(Y0)
I⁻ (μA)
0.1
0.05
(Y1)
μ⁻
π⁻
0
1.0
2.0
3.0
4.0
5.0
6.0
B_M
(×165 Gauss)

Fig. 10

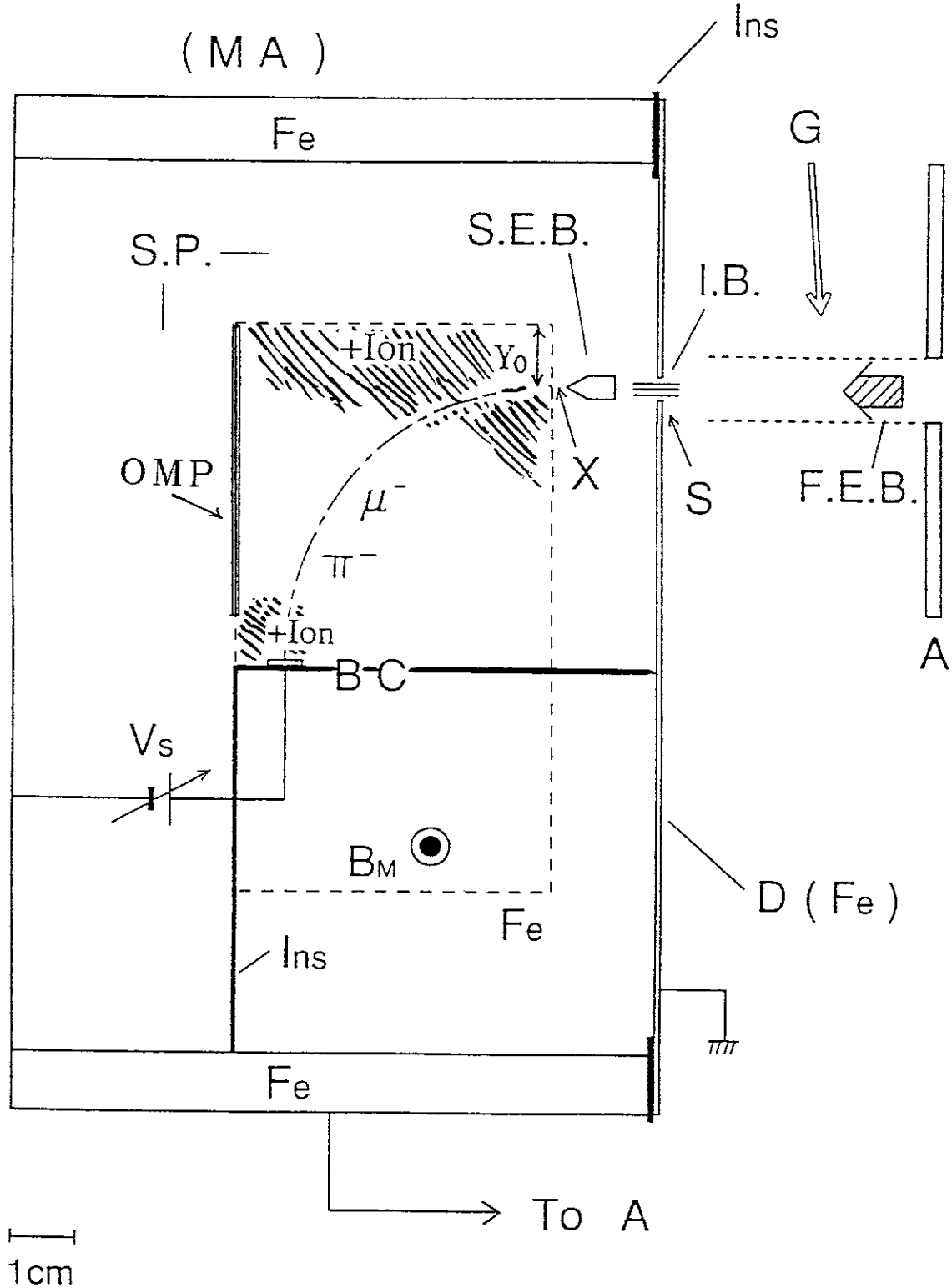
(M A)
Ins
Fe
G
S.P.
S.E.B.
I.B.
+Ion
Y0
OMP
X
S
F.E.B.
μ⁻
π⁻
+Ion
A
B-C
Vs
BM
D (Fe)
Fe
Ins
Fe
To A
1cm

Fig. 11

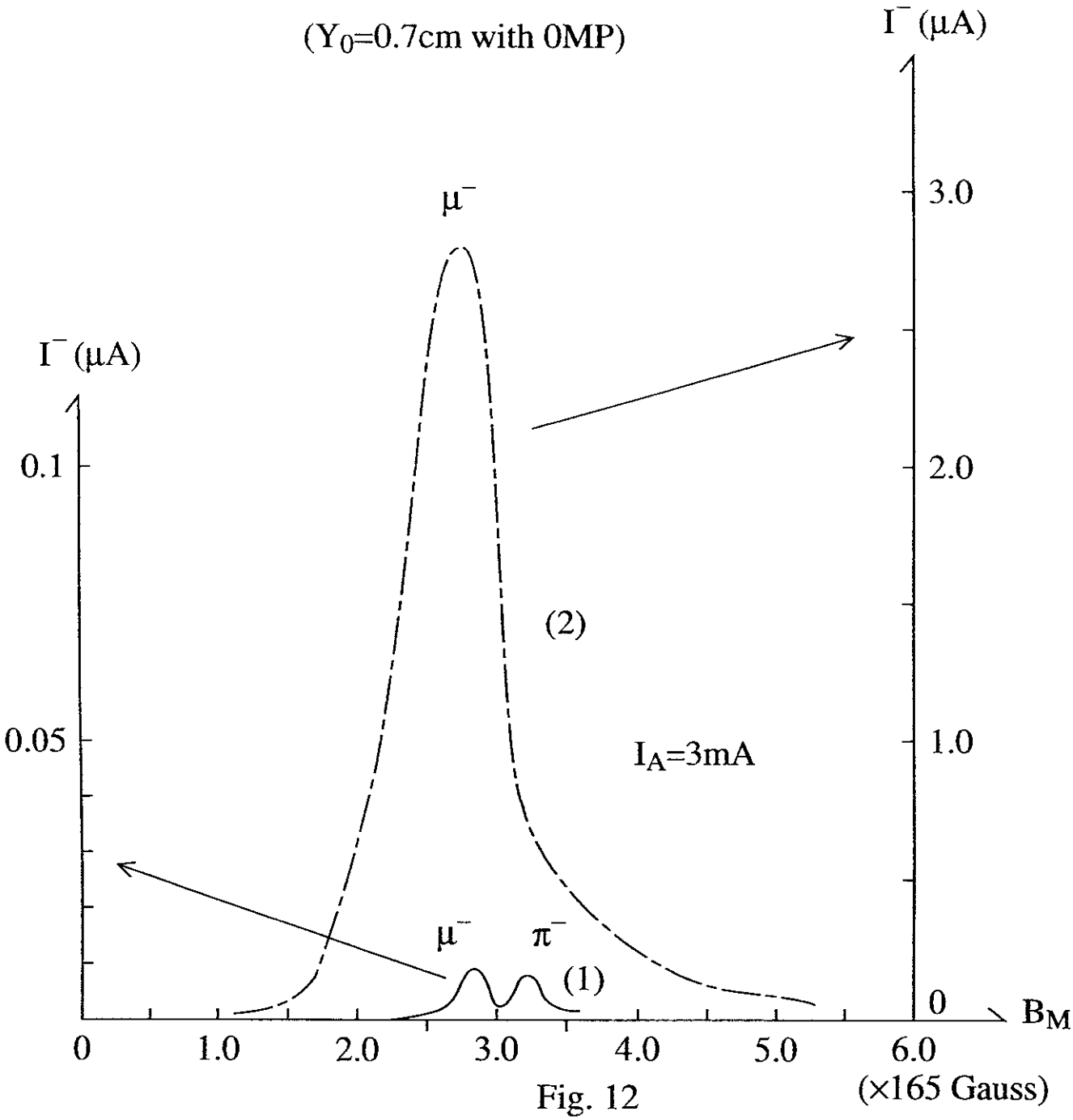
(Y_0=0.7cm with 0MP)
I^- (μA)
I^- (μA)
3.0
2.0
1.0
0
0.1
0.05
μ^-
μ^-
π^-
(1)
(2)
I_A=3mA
B_M
0
1.0
2.0
3.0
4.0
5.0
6.0
(×165 Gauss)

Fig. 12

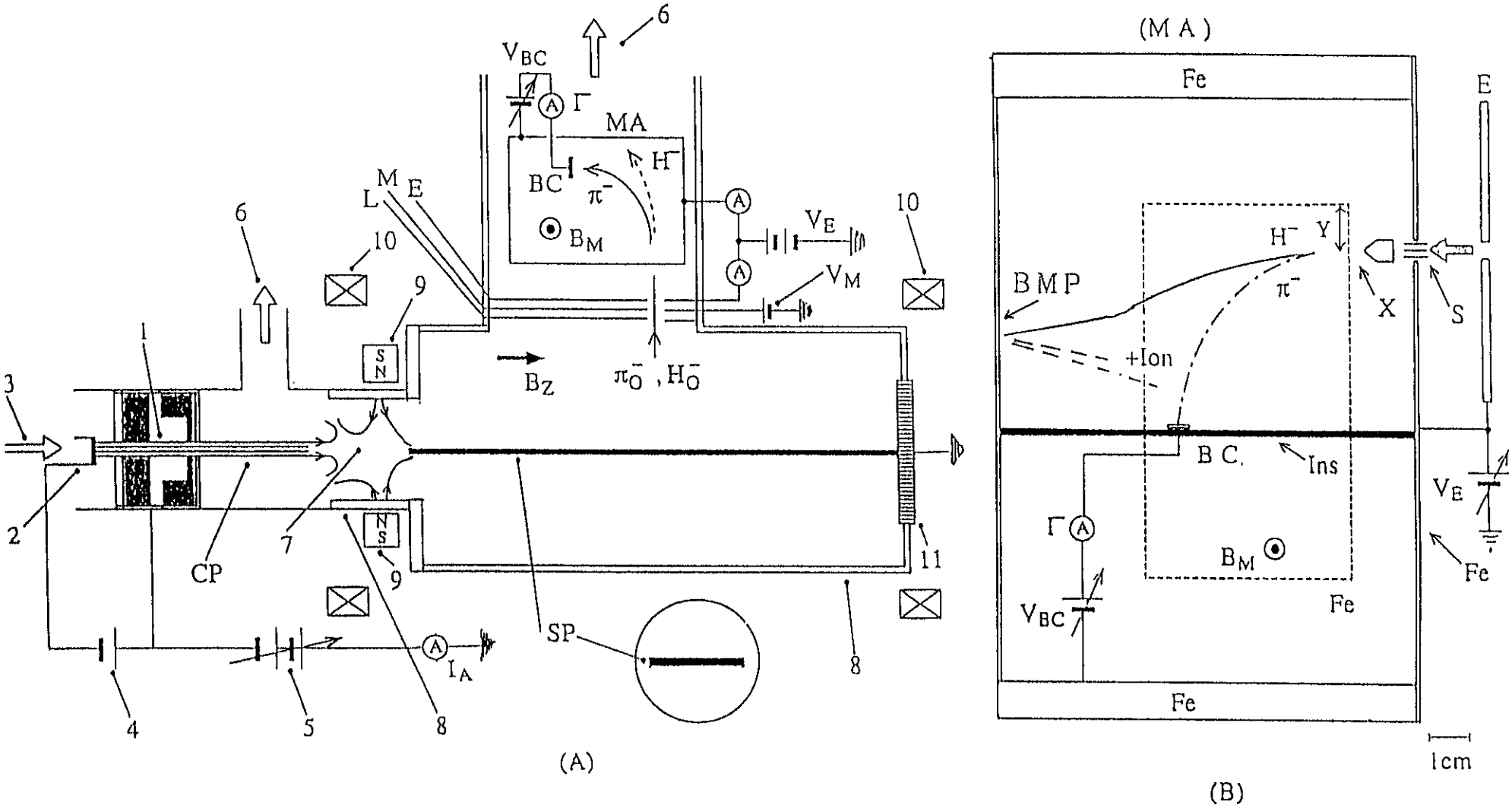
6
V_{BC}
Γ
MA
BC
H^-
π^-
B_M
M
L
E
V_E
V_M
10
9
1
3
2
CP
7
B_Z
π_O^- , H_O^-
S
N
11
8
SP
I_A
4
5
(A)
(M A)
Fe
E
BMP
+Ion
Y
X
S
B C.
Ins
Fe
1cm
(B)

Fig. A1

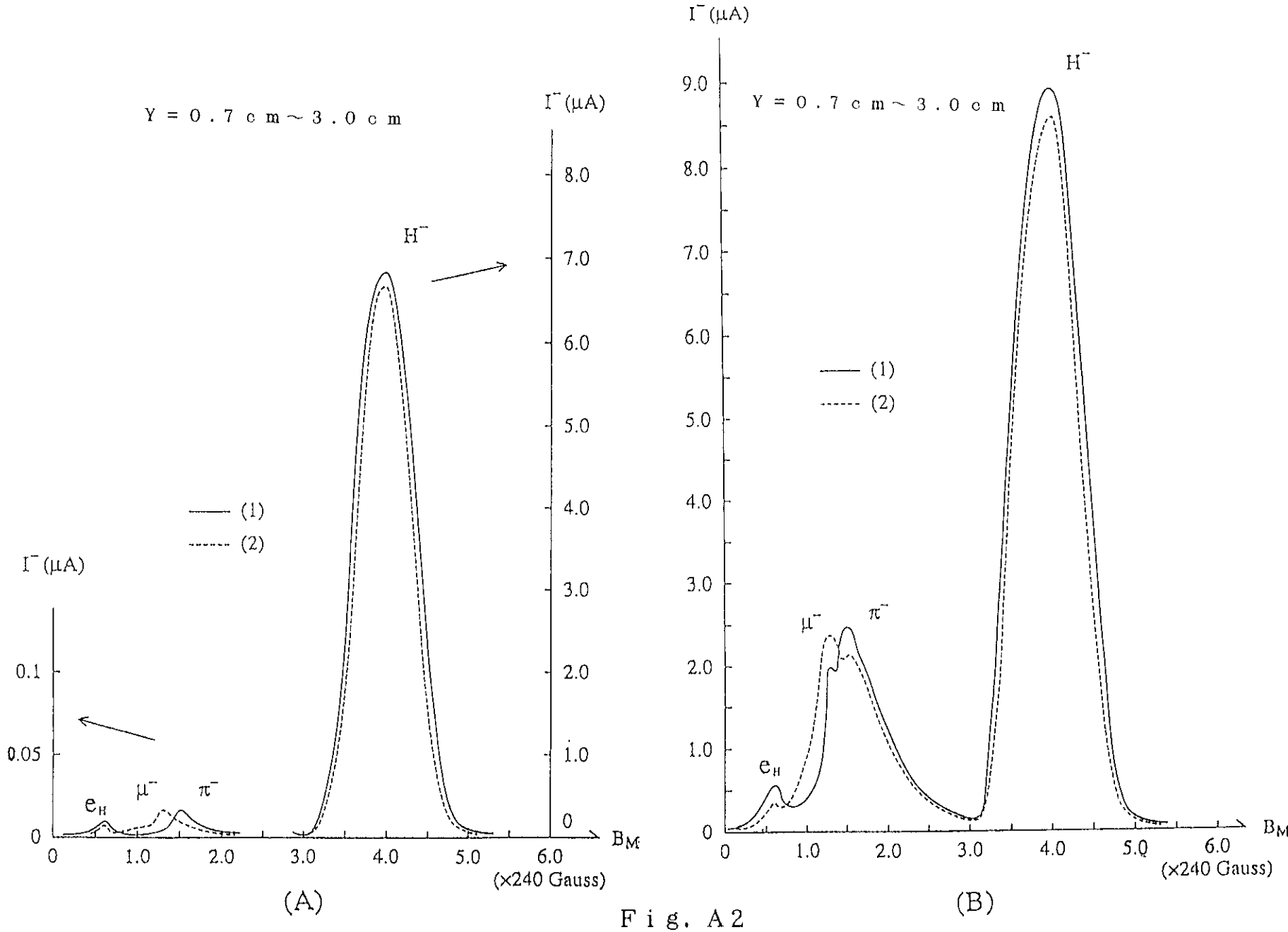

Fig. A2

Recent Issues of NIFS Series

NIFS-478 H. Sugama and W. Horton,
Neoclassical Electron and Ion Transport in Toroidally Rotating Plasmas; Jan. 1997

NIFS-479 V.L. Vdovin and I.V. Kamenskij,
3D Electromagnetic Theory of ICRF Multi Port Multi Loop Antenna; Jan. 1997

NIFS-480 W.X. Wang, M. Okamoto, N. Nakajima, S Murakami and N. Ohyabu,
Cooling Effect of Secondary Electrons in the High Temperature Divertor Operation; Feb. 1997

NIFS-481 K. Itoh, S.-I. Itoh, H. Soltwisch and H.R. Koslowski,
Generation of Toroidal Current Sheet at Sawtooth Crash; Feb. 1997

NIFS-482 K. Ichiguchi,
Collisionality Dependence of Mercier Stability in LHD Equilibria with Bootstrap Currents; Feb. 1997

NIFS-483 S. Fujiwara and T. Sato,
Molecular Dynamics Simulations of Structural Formation of a Single Polymer Chain: Bond-orientational Order and Conformational Defects; Feb. 1997

NIFS-484 T. Ohkawa,
Reduction of Turbulence by Sheared Toroidal Flow on a Flux Surface; Feb. 1997

NIFS-485 K. Narihara, K. Toi, Y. Hamada, K. Yamauchi, K. Adachi, I. Yamada, K. N. Sato, K. Kawahata, A. Nishizawa, S. Ohdachi, K. Sato, T. Seki, T. Watari, J. Xu, A. Ejiri, S. Hirokura, K. Ida, Y. Kawasumi, M. Kojima, H. Sakakita, T. Ido, K. Kitachi, J. Koog and H. Kuramoto,
Observation of Dusts by Laser Scattering Method in theJIPPT-IIU Tokamak Mar. 1997

NIFS-486 S. Bazdenkov, T. Sato and The Complexity Simulation Group,
Topological Transformations in Isolated Straight Magnetic Flux Tube; Mar. 1997

NIFS-487 M. Okamoto,
Configuration Studies of LHD Plasmas; Mar. 1997

NIFS-488 A. Fujisawa, H. Iguchi, H. Sanuki, K. Itoh, S. Lee, Y. Hamada, S. Kubo, H. Idei, R. Akiyama, K. Tanaka, T. Minami, K. Ida, S. Nishimura, S. Morita, M. Kojima, S. Hidekuma, S.-I. Itoh, C. Takahashi, N. Inoue, H. Suzuki, S. Okamura and K. Matsuoka,
Dynamic Behavior of Potential in the Plasma Core of the CHS Heliotron/Torsatron; Apr. 1997

NIFS-489 T. Ohkawa,
Pfirsch - Schlüter Diffusion with Anisotropic and Nonuniform Superthermal Ion Pressure; Apr. 1997

NIFS-490 S. Ishiguro and The Complexity Simulation Group,
Formation of Wave-front Pattern Accompanied by Current-driven Electrostatic Ion-cyclotron Instabilities; Apr. 1997

NIFS-491 A. Ejiri, K. Shinohara and K. Kawahata,
An Algorithm to Remove Fringe Jumps and its Application to Microwave Reflectometry; Apr. 1997

NIFS-492 K. Ichiguchi. N. Nakajima. M. Okamoto,
Bootstrap Current in the Large Helical Device with Unbalanced Helical Coil Currents; Apr. 1997

NIFS-493 S. Ishiguro, T. Sato, H. Takamaru and The Complexity Simulation Group,
V-shaped dc Potential Structure Caused by Current-driven Electrostatic Ion-cyclotron Instability; May 1997

NIFS-494 K. Nishimura, R. Horiuchi, T. Sato,
Tilt Stabilization by Energetic Ions Crossing Magnetic Separatrix in Field-Reversed Configuration; June 1997

NIFS-495 T. -H. Watanabe and T. Sato,
Magnetohydrodynamic Approach to the Feedback Instability; July 1997

NIFS-496 K. Itoh, T. Ohkawa, S. -I.Itoh, M. Yagi and A. Fukuyama
Suppression of Plasma Turbulence by Asymmetric Superthermal Ions; July 1997

NIFS-497 T. Takahashi. Y. Tomita, H. Momota and Nikita V. Shabrov,
Collisionless Pitch Angle Scattering of Plasma Ions at the Edge Region of an FRC; July 1997

NIFS-498 M. Tanaka, A.Yu Grosberg, V.S. Pande and T. Tanaka,
Molecular Dynamics and Structure Organization in Strongly-Coupled Chain of Charged Particles; July 1997

NIFS-499 S. Goto and S. Kida,
Direct-interaction Approximation and Reynolds-number Reversed Expansion for a Dynamical System; July 1997

NIFS-500 K. Tsuzuki, N. Inoue, A. Sagara, N. Noda, O. Motojima, T. Mochizuki, T. Hino and T. Yamashina,
Dynamic Behavior of Hydrogen Atoms with a Boronized Wall; July 1997

NIFS-501 I. Viniar and S. Sudo,
Multibarrel Repetitive Injector with a Porous Pellet Formation Unit; July

1997

NIFS-502 V. Vdovin, T. Watari and A. Fukuyama,
An Option of ICRF Ion Heating Scenario in Large Helical Device; July 1997

NIFS-503 E. Segre and S. Kida,
Late States of Incompressible 2D Decaying Vorticity Fields; Aug. 1997

NIFS-504 S. Fujiwara and T. Sato,
Molecular Dynamics Simulation of Structural Formation of Short Polymer Chains; Aug. 1997

NIFS-505 S. Bazdenkov and T. Sato
Low-Dimensional Model of Resistive Interchange Convection in Magnetized Plasmas; Sep. 1997

NIFS-506 H. Kitauchi and S. Kida,
Intensification of Magnetic Field by Concentrate-and-Stretch of Magnetic Flux Lines; Sep. 1997

NIFS-507 R.L. Dewar,
Reduced form of MHD Lagrangian for Ballooning Modes; Sep. 1997

NIFS-508 Y.-N. Nejoh,
Dynamics of the Dust Charging on Electrostatic Waves in a Dusty Plasma with Trapped Electrons; Sep.1997

NIFS-509 E. Matsunaga, T.Yabe and M. Tajima,
Baroclinic Vortex Generation by a Comet Shoemaker-Levy 9 Impact; Sep. 1997

NIFS-510 C.C. Hegna and N. Nakajima,
On the Stability of Mercier and Ballooning Modes in Stellarator Configurations; Oct. 1997

NIFS-511 K. Orito and T. Hatori,
Rotation and Oscillation of Nonlinear Dipole Vortex in the Drift-Unstable Plasma; Oct. 1997

NIFS-512 J. Uramoto,
Clear Detection of Negative Pionlike Particles from H_2 Gas Discharge in Magnetic Field; Oct. 1997

NIFS-513 T. Shimozuma, M. Sato, Y. Takita, S. Ito, S. Kubo, H. Idei, K. Ohkubo, T. Watari, T.S. Chu, K. Felch, P. Cahalan and C.M. Loring, Jr,
The First Preliminary Experiments on an 84 GHz Gyrotron with a Single-Stage Depressed Collector; Oct. 1997

NIFS-514 T. Shjmozuma, S. Morimoto, M. Sato, Y. Takita, S. Ito, S. Kubo, H. Idei, K. Ohkubo and

T. Watari,
A Forced Gas-Cooled Single-Disk Window Using Silicon Nitride Composite for High Power CW Millimeter Waves; Oct. 1997

NIFS-515 K. Akaishi,
On the Solution of the Outgassing Equation for the Pump-down of an Unbaked Vacuum System; Oct. 1997

NIFS-516 *Papers Presented at the 6th H-mode Workshop (Seeon, Germany)*; Oct. 1997

NIFS-517 John L. Johnson,
The Quest for Fusion Energy; Oct. 1997

NIFS-518 J. Chen, N. Nakajima and M. Okamoto,
Shift-and-Inverse Lanczos Algorithm for Ideal MHD Stability Analysis; Nov. 1997

NIFS-519 M. Yokoyama, N. Nakajima and M. Okamoto,
Nonlinear Incompressible Poloidal Viscosity in L=2 Heliotron and Quasi-Symmetric Stellarators; Nov. 1997

NIFS-520 S. Kida and H. Miura,
Identificaiton and Analysis of Vortical Structures; Nov. 1997

NIFS-521 K. Ida, S. Nishimura, T. Minami, K. Tanaka, S. Okamura, M. Osakabe, H. Idei, S. Kubo, C. Takahashi and K. Matsuoka,
High Ion Temperature Mode in CHS Heliotron/torsatron Plasmas; Nov. 1997

NIFS-522 M. Yokoyama, N. Nakajima and M. Okamoto,
Realization and Classification of Symmetric Stellarator Configurations through Plasma Boundary Modulations; Dec. 1997

NIFS-523 H. Kitauchi,
Topological Structure of Magnetic Flux Lines Generated by Thermal Convection in a Rotating Spherical Shell; Dec. 1997

NIFS-524 T. Ohkawa,
Tunneling Electron Trap; Dec. 1997

NIFS-525 K. Itoh, S.-I. Itoh, M. Yagi, A. Fukuyama,
Solitary Radial Electric Field Structure in Tokamak Plasmas; Dec. 1997

NIFS-526 Andrey N. Lyakhov,
Alfven Instabilities in FRC Plasma; Dec. 1997

NIFS-527 J. Uramoto,
Net Current Increment of negative Muonlike Particle Produced by the electron and Positive Ion Bunch-method; Dec. 1997